Disagreement between theory and experiment in the simplest chemical reaction: Collision energy dependent rotational distributions for $H+D_2 \rightarrow HD(\nu'=3,j')+D$

Andrew E. Pomerantz, Florian Ausfelder, and Richard N. Zare[a)]
Department of Chemistry, Stanford University, Stanford, California 94305-5080

Stuart C. Althorpe
Department of Chemistry, University of Exeter, Stocker Road, Exeter EX4 4QD, United Kingdom

F. J. Aoiz, Luis Bañares, and Jesus F. Castillo
Departamento de Química Física, Facultad de Química, Universidad Complutense, 28040 Madrid, Spain

(Received 20 August 2003; accepted 20 November 2003)

We present experimental rotational distributions for the reaction $H+D_2 \rightarrow HD(\nu'=3,j')+D$ at eight different collision energies between 1.49 and 1.85 eV. We combine a previous measurement of the state-resolved excitation function for this reaction [Ayers *et al.*, J. Chem. Phys. **119**, 4662 (2003)] with the current data to produce a map of the relative reactive cross section as a function of both collision energy and rotational quantum number (an $E-j'$ plot). To compare with the experimental data, we also present $E-j'$ plots resulting from both time-dependent and time-independent quantum mechanical calculations carried out on the BKMP2 surface. The two calculations agree well with each other, but they produce rotational distributions significantly colder than the experiment, with the difference being more pronounced at higher collision energies. Disagreement between theory and experiment might be regarded as surprising considering the simplicity of this system; potential causes of this discrepancy are discussed. © *2004 American Institute of Physics.* [DOI: 10.1063/1.1641008]

I. INTRODUCTION

The hydrogen exchange reaction has fascinated chemists for over 70 years.[1,2] Recent advances in laser techniques have allowed highly detailed measurements of this reaction:[3–11] dynamicists have succeeded in experimentally determining state-to-state integral and differential cross sections for a variety of isotopes, collision energies, and quantum states of reagents and products.[12–24] On the theoretical side, interest in this reaction derives from its simplicity. Containing only three electrons and three nuclei, this reaction lends itself to the highest level of theory.[25–28] This continually advancing theory has achieved quantitative agreement with experimental measurements of the thermal rate constant of the reaction,[26,29] inelastic scattering product state distributions,[30,31] and quantum state resolved values of reactive integral[13–18] and differential[16,19–21,32] cross sections. These successes have demanded improvement to the potential energy surface,[16,33,34] advancement in theoretical techniques,[28,35,36] and the inclusion of previously neglected effects such as geometric phase[37–39] and the Born–Oppenheimer diagonal correction.[29]

In this report we show new data on an aspect of the reaction that has received relatively little attention: the collision energy dependence of rotational distributions. This has been investigated previously at low energies,[31,40,41] but those results have been called into question.[42–44] Surprisingly, theory and experiment do not agree for this observable.

Here we present measurements of the collision energy dependence of the rotational distributions for the reaction $H+D_2 \rightarrow HD(\nu'=3,j')+D$ over the range 1.49–1.85 eV. By combining these distributions with a previous measurement of the excitation function for this reaction,[45] we are able to construct a fully experimental map of the relative reactive cross section as a function of both the collision energy and the rotational quantum number j'; we call this measurement an $E-j'$ plot. We also present $E-j'$ plots resulting from both time-dependent and time-independent fully quantum mechanical calculations. Whereas theory and experiment agree at low energy, the theoretical distributions are found to become increasing colder than the experimental ones as the collision energy increases. Finally, we perform a surprisal analysis to understand better the differences between theory and experiment, and we discuss some possible causes for this discrepancy.

II. EXPERIMENT

A. Experimental setup

We perform the experiments using a photoinitiated reaction with resonantly enhanced multiphoton ionization (REMPI) detection (see Fig. 1). A more detailed description of the apparatus has been presented recently, so we concentrate on novel aspects relevant to the current experiment.[45] A single molecular beam of 10% HBr in D_2 is introduced into a vacuum chamber through a pulsed valve. The reaction is initiated by photolyzing the HBr with tuneable UV laser

[a)]Author to whom all correspondence should be addressed. Electronic mail: zare@stanford.edu

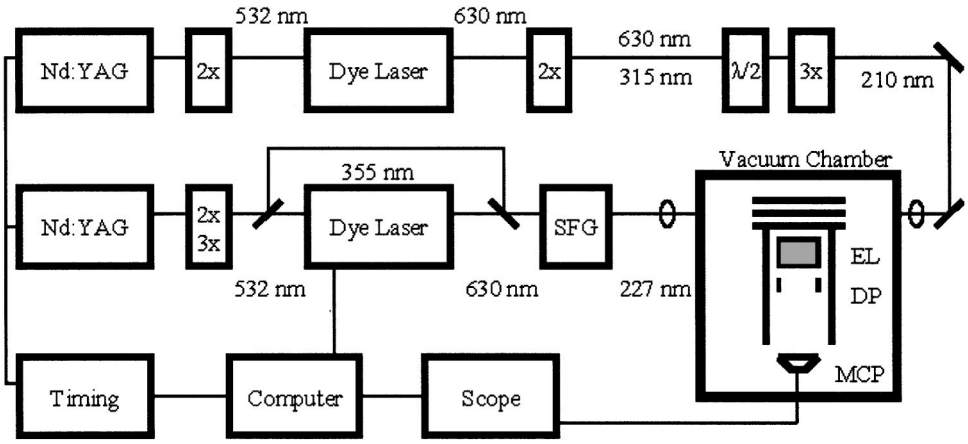

FIG. 1. Experimental block diagram: the top line depicts the tripling scheme and the middle line depicts the 355 mixing scheme. SFG is the sum frequency generation in a nonlinear optical crystal, EL is the einzel lens, and DP are the deflection plates.

light. Approximately 2 mJ of photolysis light in the range of 203–220 nm results from tripling the output of a dye laser (Quanta-Ray PDL-2) pumped by the second harmonic of a Nd:YAG laser (Quanta-Ray Cobra Laser). This photoinitiation method allows us to scan the collision energy by tuning the photolysis wavelength. Approximately 20 ns after photolysis, reaction products are probed by $2+1$ REMPI on the $E,F\,^1\Sigma_g^+ - X\,^1\Sigma_g^+$ (0,3) band (see the following). The probe beam is focused into the chamber with a lens of 40 cm nominal focal length; however, the lens position is adjusted to compensate for the wavelength-dependent index of refraction of fused silica such that the focus occurs at the same place (overlapped with the molecular beam) at all wavelengths. Because the laser bandwidth is significantly less than the Doppler bandwidth of the HD product, we must scan the laser over the Doppler profile. The ions are formed in the ionization region of a Wiley–McLaren time-of-flight mass spectrometer and are guided with an einzel lens to a pair of multichannel plates (MCPs). The resultant signal is recorded on an oscilloscope and transferred to a PC. The area under the Doppler profiles is proportional to the concentration of HD in the probed rotational state; we then convert those concentrations to relative reaction cross sections (see Sec. II C).

Light from 225 to 228 nm is required to probe HD($\nu'=3,j'$) products, and we generate that light by directly mixing red light from a dye laser (Lambda Physik LPD3000 dye laser) with the third harmonic (355 nm) of the Nd:YAG pump laser (Quanta-Ray GCR-3). This ''355 mixing'' technique allows us to produce up to 10 mJ of 225 nm light, although we typically employ only 2–3 mJ. While we correct the data for variations in probe laser power, it is desirable to keep the laser power as constant as possible over the entire range of wavelengths required to ionize each rotational state of HD($\nu=3$). To that end, we use a mixture of sulforhodamine 640 and DCM laser dyes that keeps the power constant within about 20% over the entire wavelength range. We note that the 355 mixing scheme facilitates this, because the power in the UV depends only linearly on the dye laser power, unlike in frequency-doubling or -tripling schemes.

B. Line strength factors

In order to relate the measured signal to the concentration of HD, we must know the line strengths for the Q-branch members of the $2+1$ REMPI $E,F\,^1\Sigma_g^+ - X\,^1\Sigma_g^+$ (0,3) transitions. Efforts have been made previously in this laboratory to measure those relative line strengths.[3,46–48] Unfortunately, those measurements relied on a thermal source, and the temperature required to put detectable population in the $\nu=3$ manifold proved prohibitively high; thus, no experimental data exist for this vibrational manifold. However, both experimental and theoretical values do exist for the $\nu=0$, 1, 2 manifolds of H_2, HD, and D_2. Experiment and theory agree very well, and the result is that for the lowest 15–20 rotational states in each vibrational level, the line strengths depend strongly on ν but only weakly on j.

We have performed a new experiment to measure the relative line strengths for the low-lying rotational states of HD($\nu=3$).[49] A stream of HD passed over a hot tungsten ion gauge filament is used to provide a known distribution of rovibrationally excited states of HD. This technique is known to create HD molecules that are vibrationally excited but rotationally relaxed such that they can be well-described by a Boltzmann distribution slightly above room temperature.[50–53] To calibrate the line strengths, we scan over each observable line; we can detect population in states $j \leqslant 4$. Figure 2 presents a Boltzmann distribution derived from those scans with the assumption that the area under the scan gives the relative population in each state without any correction, i.e., assuming that all line strengths are unity. This plot reveals a thermal population of HD with temperature of 302 ± 9 K. The fact that we can accurately measure populations of HD states in this thermal sample without needing to apply a correction factor means that we should be able to measure populations of HD states produced by a reaction without needing any further corrections.

There are also recent calculations of these line strengths[54] performed with the same theoretical methodology as in previous work.[47,48] As with the other isotopes and vibrational manifolds, and in agreement with these measure-

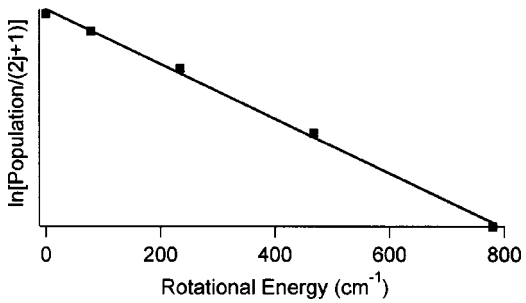

FIG. 2. Boltzmann plot of vibrationally excited HD($\nu'=3$) produced by the ion gauge filament. The squares are the experimental measurements and the line is the fit to a Boltzmann distribution, yielding a rotational temperature of 302 ± 9 K.

ments of the low-lying rotational states, the calculations show that the line strengths depend only weakly on the initial rotational state; the line strengths increase monotonically with j, but the difference between the strongest and weakest lines we detect in the rotational distribution measurements is only 10%. We correct the measured signals using these theoretical line strengths in analyzing the rotational distributions, but this correction is quite small because the line strengths are so similar.

C. Converting measured concentrations to relative cross sections

Knowledge of the rotational line strengths allows us to convert the areas under the Doppler scans to the relative concentrations of HD(ν',j') product. But we still must convert these concentrations into relative cross sections for production of the different product state. In this photoinitiated experiment, relative partial cross sections are related to product concentration according to[45,55]

$$\sigma(\nu',j')=\frac{n_{\mathrm{HD}}(\nu',j')}{n_{\mathrm{H}}n_{\mathrm{D_2}}}\frac{1}{\nu\cdot\Delta\tau}, \tag{1}$$

where n_x is the concentration of species x, ν is the relative velocity of the reagents, and $\Delta\tau$ is the time delay between initiation and detection. Here we have assumed that the reagents are not depleted during the short (20 ns) time between initiation and detection. If we keep $n_{\mathrm{D_2}}$, n_{H}, ν, and $\Delta\tau$ constant during the course of the experiment (i.e., while scanning all j' lines), then the relative partial cross sections are given simply by the concentrations $n_{\mathrm{HD}}(\nu',j')$. We believe $n_{\mathrm{D_2}}$ is constant because we use the same gas mixture and have the same expansion at roughly the same backing pressure throughout a rotational distribution measurement. For a given collision energy we also believe that n_{H} is constant. This quantity depends on the concentration of HBr in the molecular beam and on the characteristics of the photolysis laser. We assume the concentration of HBr to be constant, and the photolysis conditions do not change significantly while measuring a rotational distribution at a single collision energy. On the other hand, the photolysis conditions do change between collision energies, preventing us from easily combining the rotational distributions to produce an $E-j'$ plot. However, that effect was accounted for during a previous measurement of the excitation function of $\mathrm{H}+\mathrm{D_2}\rightarrow\mathrm{HD}(\nu'=3,j'=0)+\mathrm{D}$;[45] thus, we can combine that result with the current rotational distributions to produce an $E-j'$ plot. The relative velocity of the reagents, ν, is constant for a given collision energy. The time between triggering the photolysis and probe lasers, $\Delta\tau$, is kept constant throughout each measurement.

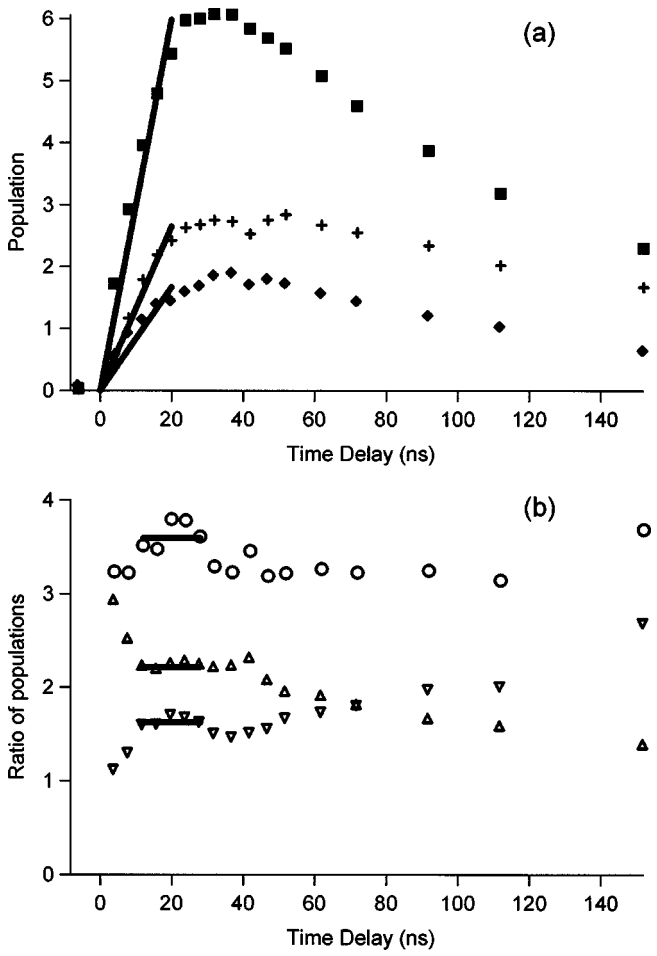

FIG. 3. Time delay studies at 1.85 eV collision energy: (a) measured populations for three product states as a function of time delay. (+) $j'=2$, (■) $j'=6$, and (♦) $j'=9$. The solid lines represent linear fits for time delays ≤20 ns and indicate that the concentrations grow linearly in time for delays up to 20 ns. (b) Ratios of these populations as a function of time delay. (▽) $(j'=2)/(j'=9)$, (△) $(j'=6)/(j'=2)$, and (○) $(j'=6)/(j'=9)$. The solid lines indicate the invariance of the ratios over the range of time delays 12–28 ns.

We must note that this expression relating concentration to partial cross section holds only under the assumption that the measured concentration is proportional to the amount of product produced by the reaction. This assumption is valid only for small values of the time delay $\Delta\tau$ between initiation and detection.[45] While allowing longer times for products to accumulate can result in larger signal, we must be careful to probe the products before their high velocities carry them outside the small focal volume of the probe laser. To verify that the data are not affected by product fly-out, we must probe in a regime in which the concentration of products grows linearly with time. Figure 3(a) presents measured concentrations for three different $\nu'=3$ product states (j'

$=2,6,9)$ as a function of $\Delta\tau$. The measured concentrations appear to grow linearly with time for approximately 20 ns after initiation, indicating that product fly-out is minimal for time delays below 20 ns. After 20 ns, the signal plateaus as fly-out competes with product buildup and eventually decays as fly-out dominates. Included in Fig. 3(a) are linear fits for time delays $\leqslant$20 ns, demonstrating the linear growth of concentrations for 20 ns.

Figure 3(b) presents time-dependent ratios of concentrations of those states; these ratios of populations are exactly the quantities measured in a rotational distribution measurement. We observe that the measured ratios are surprisingly insensitive to the time delay. The solid lines in Fig. 3(b) indicate the averages of each population ratio for time delays of 12–28 ns. In this time range we see only small deviations of the ratios, demonstrating the insensitivity to time delay. Indeed, the ratios seem unchanged even at 40 ns time delay. By that time, Fig. 3(a) shows that products are no longer building up linearly with time; thus, significant fly-out occurs at this time delay. The reason the ratios are nearly unchanged even when significant fly-out occurs is that the reaction products fly out of the probe volume at similar rates for each product state. We note that in this experiment, the speed of a reaction product in the lab frame depends not only on the collision energy and product internal excitation but also on the scattering angle; backscattered products have small lab frame speeds while forward scattered product have large lab frame speeds. It has been observed previously for this reaction that products with little rotational excitation tend to be backscattered and that the average scattering angle shifts toward forward scattering as j' increases.[17] Although the maximum energetically allowed speed is greater for low j' products, those products have low speeds in the lab frame because they are backscattered. As j' increases, the maximum energetically allowed speed decreases, but the scattering angle shifts toward forward scattered, keeping the lab frame speed roughly constant. Indeed, speed distributions have been measured for many of these products at these collision energies,[20,45] and the products' lab frame speed does not monotonically increase or decrease with j'. This behavior is in marked contrast to that which occurs in crossed molecular beams.

This experimental insensitivity to time delay is fortuitous, as the ratios of concentrations would change significantly with time delay if the product's lab frame speeds were different. Thus, we probe at small time delays (20 ns) where fly-out is not relevant and the measured concentration is independent of lab frame speed. This discussion merely serves to emphasize that small errors in the time delay do not have significant effects on the measured rotational distributions. Also, we note the biggest deviations of the ratios occur for small time delays. As can be seen in Fig. 3(a), those points are ratios of two small numbers and thus are quite sensitive to random noise. Because those time delays are in the region in which products build up linearly in time, it is quite unlikely that those deviations are due to any systematic error. Finally, it is possible for light from the probe laser to photolyze HBr, resulting in a small signal from products that have accumulated during the laser pulse. This contribution [represented by the population at negative time delay in Fig. 3(a)] was ignored as it was found to be at least an order of magnitude smaller than the signal arising from reactions initiated by the photolysis laser.

We also must verify that all the HD ions reach the detector and that no bias exists toward detection of a particular laboratory frame speed. In particular, we worry that very fast moving products might fly so far off the time-of-flight axis that they miss the MCP detector. In order to collect all the product ions, we use an einzel lens to guide the ions onto the MCPs. Using the ion optics simulation program SIMION,[56] we have calculated ion trajectories to verify that all ions should impinge on the detector. We have also performed two tests to verify that all HD ions are detected. Both of these checks were done at the highest collision energy, which is associated with the fastest moving products; checks at this collision energy should therefore provide the most stringent tests of the collection efficiency. The first check involves rotating the polarization of the photolysis laser from parallel to perpendicular to the time-of-flight axis. H atoms resulting from HBr photolysis are produced spatially anisotropically, with most H atoms distributed according to $\beta=-1$.[57] This anisotropy carriers over to the reaction products, so rotating the polarization results in a change in the laboratory frame velocity distribution. We have verified that the measured signal does not depend on the laser polarization, consistent with the collection of all ions. In addition, the time-of-flight apparatus is equipped with deflection plates between the einzel lens and the detector to help steer the ions onto the center of the MCP detector (Fig. 1). The signal we observe is insensitive to the steering voltages over a large range, again consistent with uniform detection efficiency. Therefore, we believe that we collect all ions and are able to relate the detected signal to the density of products in a particular quantum state. We note that rotating the polarization allows us to check that any possible alignment of the D_2 molecules in the mild expansion does not bias the experiment. If the D_2 were aligned, changing the polarization would switch between favoring head-on versus favoring side-on collision; the fact that the signal is independent of the laser polarization indicates that the experiment is not adversely affected by possible D_2 alignment.

Finally, we mention that the $HD(\nu'=3,j'=5,8)2+1$ REMPI lines occur near atomic bromine resonances. Space charge from Br^+ ions makes it difficult to resolve masses when the probe laser lies on one of these bromine lines. Fortunately, the line centers are far enough apart that the bromine signal has returned to baseline at the center of the HD lines in question. To measure those populations, we integrate the uncontaminated half of the HD Doppler profile and then double that area; for the other states, we simply integrate the entire Doppler profile. We believe that this method does not introduce systematic error into the measurement of these populations, although integration of only half of the line does result in increased random error. Thus, we believe that the conditions do not change significantly during a measurement, the products we measure are not affected by fly-out, the signal is not contaminated by signal arising from the probe laser only, and all the ionized molecules impinge

upon the detector. Hence, we believe we can safely relate the measured HD(ν',j') concentrations to relative reactive cross sections. The above may seem belabored; we would not have presented such an elaboration were it not for the disagreement with theory (see the following).

III. THEORETICAL METHODS

These experimental results are compared to time-dependent and time-independent calculations. All calculations used the Boothroyd-Keogh-Martin-Peterson surface II (BKMP2) potential energy surface (PES)[33] and were confined to the ground surface, neglecting all non-Born–Oppenheimer correction terms (such as the geometric phase effect).

A. Time-dependent quantum mechanical method

The time-dependent wave packet results were obtained using the method of Ref. 58, in which a quantum wave packet, containing a spread of energies, is propagated from the initial $A+BC$ ($H+D_2$) through to the final $AC+B$ ($HD+D$) arrangements of the reaction.[58] Efficient basis sets are constructed from grids based on $A+BC$ Jacobi coordinates in the reagent approach region, and $AC+B$ coordinates in the transition-state and product exit regions. This method recently yielded the first rovibrationally state-to-state resolved cross sections to be calculated by time-dependent wave packet methods,[58] and has since been applied to several reactions.[20,32] The $H+D_2(\nu=0,j=0)\rightarrow HD(\nu'=3,j')+D$ cross sections were obtained by propagating wave packets for all values of the total angular momentum quantum number J between 0 and 30. The basis function grids used were sufficiently dense to converge individual fixed-J reaction probabilities to better than 2%, over a continuous range of collision energies from $E_{\mathrm{coll}}=0$ to 2.2 eV.

B. Time-independent quantum mechanical method

The time-independent quantum mechanical (QM) calculations were performed for the $H+D_2(\nu=0,j=0)$ reaction by means of a time-independent coupled-channel hyperspherical method[59] at the collision energies measured experimentally over the range 1.49–1.85 eV. The key parameters that define the coupled-channel basis set are $E_{\max}$, $j_{\max}$, and $k_{\max}$ (see Ref. 59). At the collision energies of the present work, well converged integral cross sections were obtained using the parameters $j_{\max}=20$, $E_{\max}=2.85$ eV, and $k_{\max}=10$ and including all partial waves up to total angular momentum $J=36$. Using these parameters, the number of channels to be propagated ranges from 198 at $J=0$ up to 1532 at $J\geqslant 10$. A maximum value of the hyperradius $\rho_{\max}=2.5\ a_0$ and 250 sectors were selected to perform the calculations.

C. Quasiclassical trajectory method

In addition to the above-mentioned QM calculations, quasiclassical trajectory (QCT) calculations were performed for the $H+D_2(\nu=0,j=0,1,2)$ reactions on the same BKMP2 PES at 1.64 and 1.85 eV collision energies to check for the effect of the internal energy of the D_2 reagent on the product HD($\nu'=3$) rotational distributions. The QCT method employed in this work has been described elsewhere,[60] and only the details relevant to the present work are given here. Batches of 10^6 trajectories were run at each collision energy and initial rotational quantum state of the D_2 reagent. Trajectories were started at a H–D_2 distance of 7 Å and a time step of 5×10^{-17} s was used; this guarantees conservation of the total energy to better than one part in 10^5 and conservation of total angular momentum to better than one part in 10^6. The maximum impact parameter employed was 1.35 Å in all cases. The rovibrational energies of the D_2 and HD molecules were calculated by semiclassical quantization of the classical action, using in each case the asymptotic diatomic potential of the PES.[60] The assignment of the final product quantum numbers was carried by equating the classical rotational angular momentum of the product molecule to $[j'(j'+1)]^{1/2}\hbar$. With the (real) j' value so obtained, the (real) vibrational quantum number ν' is found by equating the internal energy of the outgoing molecule to the corresponding Dunham expansion. As in recent works,[61] we have implemented both Gaussian-weighted and histogramatic binning procedures for the final assignment of integer ν' and j' values. As was discussed in Refs. 60 and 61, Gaussian-weighted binning is expected to be superior when the QCT results are compared with available QM calculations.

IV. RESULTS

Figure 4 presents experimental rotational distributions for the reaction $H+D_2\rightarrow HD(\nu'=3,j')+D$ for eight different collision energies between 1.49 and 1.85 eV. We estimate a spread in collision energy of approximately 0.05 eV,[62] so we space the measurements by that amount. While these collision energies are high, the product states have so much energy in vibration that these channels are close to the energetic threshold. At the lowest collision energy, the highest energetically allowed rotational state is $j'=5$, whereas at the highest energy it is $j'=10$ (see Table I). Thus, by scanning the collision energy, we are able to observe how population grows into states that are inaccessible at the low energies.

We can offer one additional check on the experimental data. Using a similar experimental setup, Bean *et al.*[18] measured the HD($\nu'=3,j'$) product state distribution at a single collision energy (1.64 eV). Figure 5 presents a comparison of these earlier results with the present experimental data. The close agreement gives us further confidence in the present experimental procedure and analysis.

The rotational distributions in Fig. 4 can be combined with a previous measurement[45] of the excitation function for the reaction $H+D_2\rightarrow HD(\nu'=3,j'=0)+D$ to produce a map of the relative reactive cross section as a function of collision energy and rotational quantum number (an $E-j'$ plot). This is possible because the excitation function yields the relative partial cross section for forming HD($\nu'=3,j'=0$) product over a range of collision energies and the rotational distributions relate partial cross sections for forming HD($\nu'=3,j'\neq0$) to the HD($\nu'=3,j'=0$) cross section at each energy. Figure 6 presents experimental and theoretical $E-j'$ plots for the reaction $H+D_2\rightarrow HD(\nu'=3,j')+D$ between 1.49 and 1.85 eV collision energy. Figure 6 and Fig. 4 constitute the central results of this study.

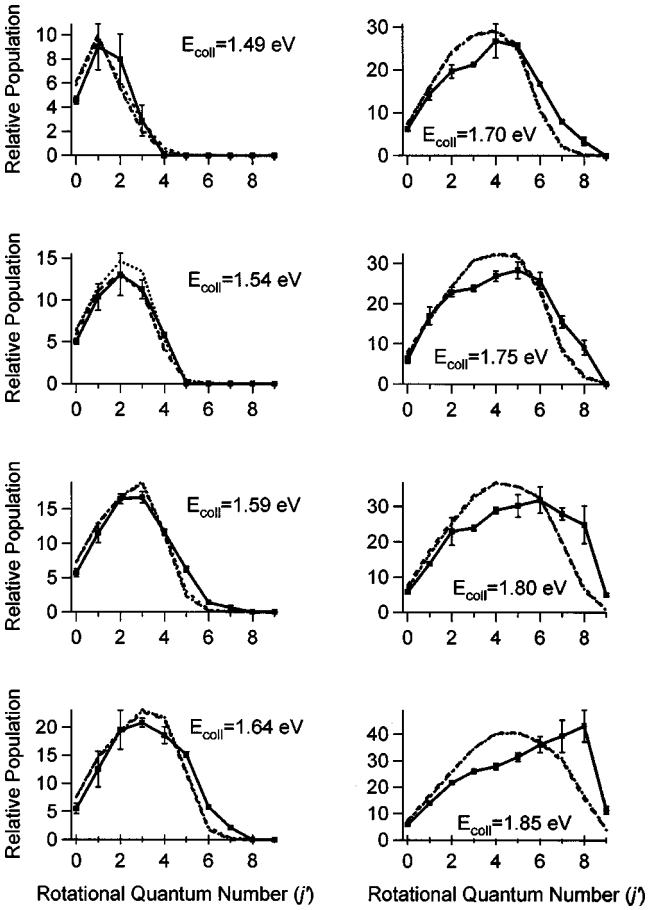

FIG. 4. Experimental and theoretical rotational distributions for the title reaction over a range of collision energies. Closed squares represent experimental data points; error bars are statistical and represent 95% confidence intervals. Dashed lines represent time-independent QM calculations, dotted lines represent time-dependent QM calculations, and dash-dot lines represent time-dependent QM calculations including the experimental spread in collision energy. For most collision energies, the theoretical distributions are indistinguishable.

One potential complication in the interpretation of these experimental results is the presence of two distinct collision energies at every photolysis wavelength. HBr photolysis at these wavelengths can proceed via two channels, $HBr+h\nu \rightarrow H+Br$ and $HBr+h\nu \rightarrow H+Br^*$, where Br* denotes spin–orbit excited Br.[57] We call the H+Br* photolysis channel the slow channel, as the H atoms move slowly because the energy required to excite Br is unavailable for H-atom translation; similarly we call the H+Br photolysis channel the fast channel. At the higher collision energies, slow H atoms have enough energy to populate $HD(\nu'=3)$, and the present experiment has no means by which to resolve reactions result-

TABLE I. Potential contributions of the slow channel to the measured rotational distributions. Dashes "-" indicate that the slow channel is energetically forbidden from populating any $HD(\nu'=3,j')$ states.

E_{coll} (eV) fast channel	E_{coll} (eV) slow channel	Max slow contribution	j'_{max} fast channel	j'_{max} slow channel	j'_{max} observed
1.49	1.13	-	5	-	3
1.54	1.18	-	6	-	4
1.59	1.23	-	7	-	7
1.64	1.28	-	7	-	7
1.70	1.34	1%	8	1	8
1.75	1.39	2%	9	3	8
1.80	1.44	9%	9	4	9
1.85	1.49	13%	10	5	9

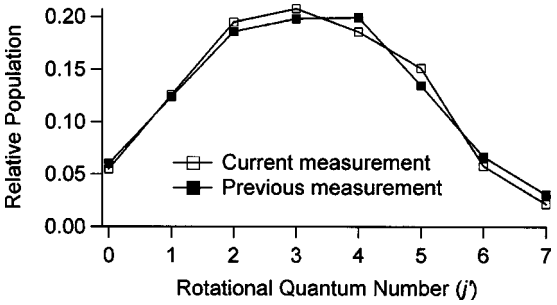

FIG. 5. Comparison of the present $HD(\nu'=3,j')$ distribution against an earlier measurement (Ref. 18) at 1.64 eV collision energy.

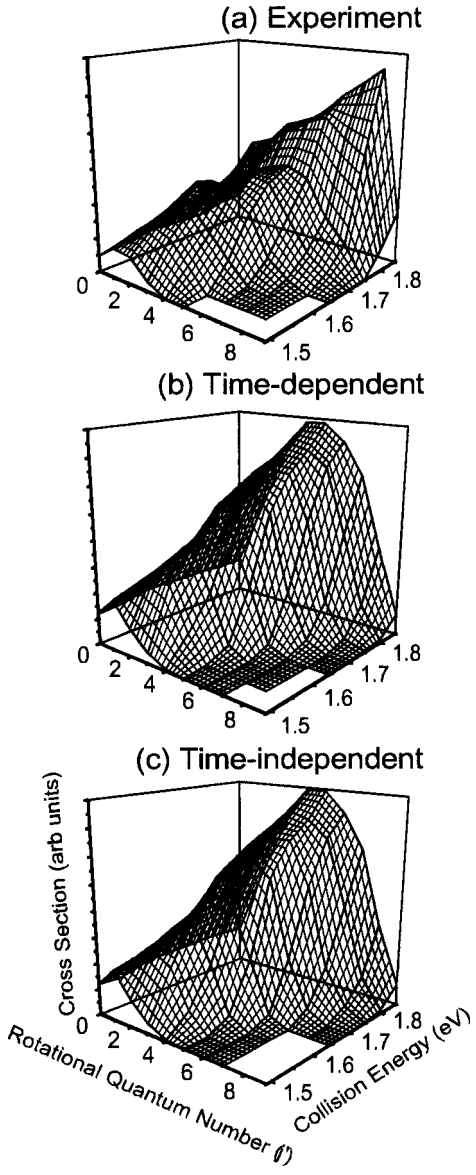

FIG. 6. $E-j'$ plots from (a) experiment, (b) time-dependent QM calculations, and (c) time-independent QM calculations.

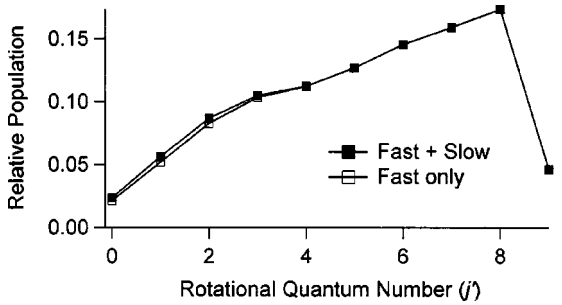

FIG. 7. The HD($\nu'=3,j'$) distribution at 1.85 eV collision energy with and without subtraction of the contribution from the slow channel. (■) The measured rotational distribution and (□) the same distribution after removing the contribution from the slow channel.

ing from fast versus slow H atoms. Although the experimental results are contaminated with products from the slow-channel reaction, we argue here that this effect is small. For the four lowest collision energies, the slow-channel reaction is below the energetic threshold for populating HD($\nu'=3$). For the higher collision energies, there are three reasons why this experiment is heavily biased against the slow channel. The first is the branching ratio: there are more fast H atoms produced by approximately 6:1.[57] The second is that the slower-moving H atoms experience fewer collisions than the faster-moving H atoms during the same time delay, resulting in fewer reactive events. The third is the lower reactive cross sections at lower collision energies.

The effect of the slow-channel reactions is that the measurement overestimates the amount of population of the low j' states at high collision energies, where the low j' states are populated by both channels but the high j' states are populated by the fast channel only. With knowledge of the branching ratio, collision frequency, and cross sections, we can estimate the extent of the slow channel's contribution to the measured signal. In Table I, we have used the calculated cross sections to determine the percent contribution of the slow channel to the measured signal; we report the contribution in the $j'=0$ state, as that state has the largest degree of contamination and therefore represents an upper limit to the slow channel's contribution. For the highest collision energy measured, 1.85 eV, the slow-channel reaction has a collision energy of 1.49 eV, an energy that we have also measured. Thus, we can use these measured cross sections to subtract the slow channel's contribution to the rotational distribution. Figure 7 presents rotational distributions at 1.85 eV with and without removing the slow channel. While the population in the low j' states decreases upon making this correction, the extent of the contamination is quite small.

We also compare the experimental data to time-dependent and time-independent quantum calculations (Fig. 4). At each energy the rotational distributions are normalized such that the integrated areas under all distributions are equal. The time-dependent calculations readily provide cross sections at many closely spaced energies, which allows us to simulate the collision energy broadening present in the experiment (≈50 meV). Thus, Fig. 4 presents time-dependent calculations with and without including the effects of collision energy spread; the effect is minor at all energies other

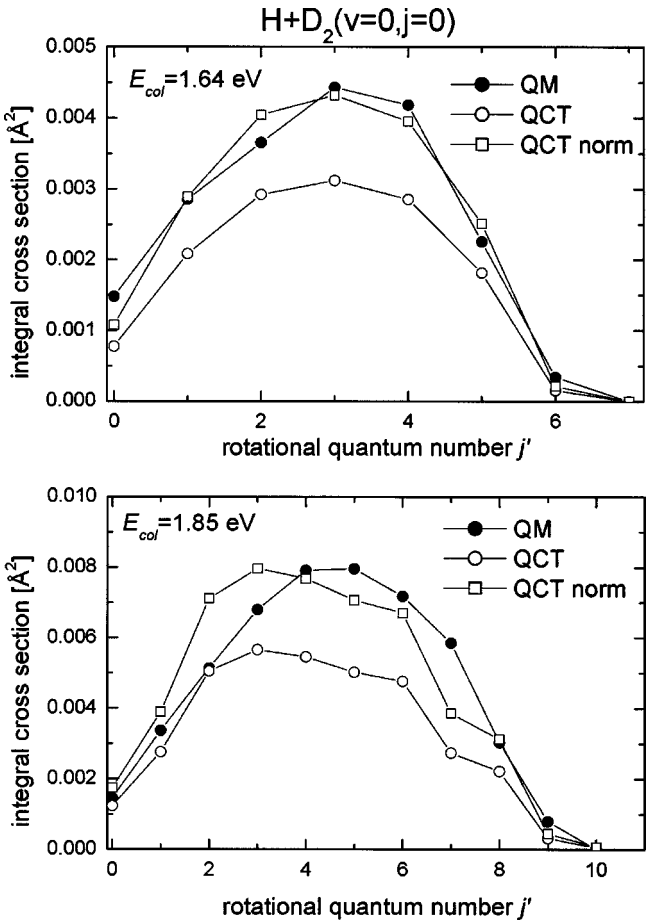

FIG. 8. Comparison between QCT and time-independent QM rotational distributions for the $H+D_2(\nu=0,j=0)$ reaction at 1.64 eV collision energy (top panel) and 1.85 eV (bottom panel). (●) The time-independent QM result, (○) the Gaussian-weighted binned QCT result, and (□) the QCT distribution normalized to have the same area as the QM one.

than 1.54 eV. A disagreement at this energy is interesting because previous measurements of differential cross sections for the reaction $H+D_2\rightarrow HD(\nu'=3,j'=0)+D$ showed poor agreement at this energy and good agreement at other energies.[20,45] Figures 6(b) and 6(c) show $E-j'$ plots constructed from both time-dependent and time-independent QM calculations. As can be seen in both the rotational distributions and the $E-j'$ plots, theory appears to agree with experiment at low energies but the calculated HD($\nu'=3,j'$) rotational distributions become increasingly too cold at high energies.

A complication of the present comparison between theory and experiment is that the D_2 molecules in the molecular beam possess a thermal distribution of rotational states whereas the QM calculations have been performed for the reaction with D_2 in $j=0$ only. We estimate that the thermal distribution corresponds to a rotational temperature of $T_{rot}\approx 90$ K (significant population in $j=0$, 1, and 2).[62] We have performed QCT calculations for all three initial rotational states of the D_2 reagent at the collision energies of 1.64 and 1.85 eV in an attempt to model more appropriately the experimental conditions. These calculations employ the Gaussian-weighted binning procedure to assign quantum states to the nascent HD product molecules. This Gaussian-

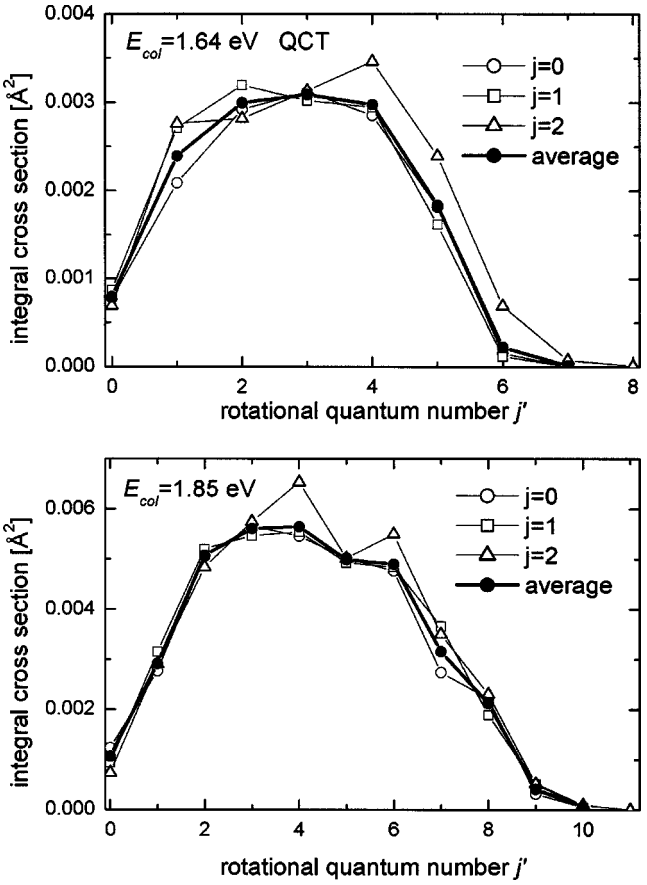

FIG. 9. QCT rotational distributions obtained by using the Gaussian-weighted binning procedure for the $H+D_2(\nu=0,j=0,1,2)$ reactions at 1.64 eV collision energy (top panel) and 1.85 eV (bottom panel). The closed circles and thick lines represent the $HD(\nu'=3)$ rotational distributions obtained by averaging over the D_2 rotational population at $T_{rot}=90$ K (populations of 0.52:0.33:0.15 for the $j=0$, 1, 2 levels, respectively).

weighted binning procedure has proved to yield rotational distributions in good agreement with the QM counterparts for reaction channels which are energetically thermoneutral or slightly endothermic or exothermic,[61] as in the present case; in contrast, the traditional histogramatic binning procedure usually yields hotter rotational distributions.[13,15,17,18,61] Figure 8 shows a comparison between the QCT Gaussian-weighted binned rotational distributions and the corresponding time-independent QM ones for the $H+D_2(\nu=0,j=0)$ reaction at 1.64 and 1.85 eV collision energies. Because the reaction cross sections predicted by the QCT method are somewhat smaller than the corresponding QM cross sections, the QCT rotational distributions have been normalized to have the same area as the QM rotational distributions. As can be seen, there is a very good agreement between the present normalized QCT rotational distributions and the QM ones at both collision energies studied. This comparison supports the validity of the QCT method in conjunction with the Gaussian-weighted binning procedure to obtain reliable rotational distributions for this system. Figure 9 depicts the QCT $HD(\nu'=3)$ rotational distributions obtained for the reaction with $D_2(j=0,1,2)$ along with the rotational distributions averaged over the initial rotational states of D_2 according to the populations at $T_{rot}\approx 90$ K. The effect of D_2 rotation on the resulting rotational distributions is quite small; moreover, the rotationally averaged distributions at both collision energies are practically indistinguishable from those obtained for the reaction with initial $j=0$. Therefore, we conclude from these QCT results that the population of $D_2(j>0)$ in the molecular beam can be ruled out as an explanation why the QM distributions are colder than the experimental ones.

V. DISCUSSION

As shown in Fig. 6(a), we have constructed a fully experimental $E-j'$ plot for the reaction $H+D_2 \rightarrow HD(\nu'=3,j')+D$ over the collision energy range 1.49–1.85 eV. We have also presented an $E-j'$ plot resulting from a fully time-dependent quantum mechanical calculation [Fig. 6(b)], which agrees closely with a time-independent quantum mechanical calculation [Fig. 6(c)]. We observe a systematic disagreement between theory and experiment at high collision energies. This result is unexpected in light of the previous good agreement found between measured and calculated rotational distributions for this reaction for many isotopes and vibrational manifolds at lower collision energies.[5,13–18,37–39,46,63–66]

In an attempt to understand these distributions, we begin by applying some traditional analyses. As is expected, the relative population of high lying rotational states increases with the collision energy. To quantify this effect, we calculate the rotational temperature, the average rotational energy, and the fraction of total energy in rotation for each rotational

TABLE II. Experimental and theoretical rotational temperatures, average energy in rotation, and fraction of energy in rotation as a function of collision energy.

	Rotational temperature (K)		Average energy in rotation (cm^{-1})		Fraction of total energy in rotation (%)	
E_{coll} (eV)	Experiment	Theory	Experiment	Theory	Experiment	Theory
1.49	288	238	160	160	1.2	1.2
1.54	540	486	299	276	2.1	2.0
1.59	766	671	459	376	3.2	2.6
1.64	1039	905	610	507	4.1	3.4
1.70	1458	1162	839	657	5.5	4.3
1.75	1695	1419	974	810	6.2	5.2
1.80	2231	1690	1257	969	7.8	6.0
1.85	2645	1953	1458	1124	8.9	6.8

distribution. Table II presents these results for the experimental and theoretical data. It is found that for the experimental distributions the rotational temperature (obtained by a Boltzmann fit to the rotational distribution) increases by a factor of 9.2, the average energy in rotation increases by a factor of 9.1, and the fraction of energy in rotation increases by a factor of 7.5 over this collision energy range. The theoretical distributions display the same trend, although the changes over this energy range are less dramatic. The fractions of energy in rotation are all low, as 75% of the total energy is required to place three quanta in vibration, even at the highest collision energy.

Valentini and co-workers[67,68] have developed a model in which a kinematic limit is imposed upon chemical reactions. Their model asserts that the skew angle (which depends only on the masses) limits the amount of energy that is available to go into internal degrees of freedom. This limit originates from the need for reactive trajectories to move with a minimum velocity along the reaction coordinate in order to enter the product valley; that minimum velocity depends solely on the skew angle. This model has been successfully applied to several reactions, explaining why many energetically allowed product states receive only a very small amount of population.[67,68] In particular, this kinematic limit correctly models the hydrogen exchange reaction for many isotopic combinations over a range of low collision energies.[67] Unexpectedly, we see significant population in states that are forbidden by this kinematic limit. Indeed, this limit forbids the population of any HD($\nu'=3,j'$) states at the lower energies, whereas we observe population in j' states up to the energetic limit at many collision energies. While this kinematic limit appears to be violated for the HD($\nu'=3$) channel, this channel results from a small percentage of the reactive collisions. Consequently, the kinematic model as applied to all reaction products may be more valid than it seems here.

A surprisal analysis has also been carried out on these rotational distributions. The surprisal analysis is an information theoretical technique that measures the extent to which a chemical reaction populates states in a statistical manner.[69,70] In applying this treatment, we employ the standard equation

$$I(j')=-\ln\left[\frac{P(j')}{P^0(j',E_{\text{avail}})}\right], \tag{2}$$

where $P(j')$ is the measured population of each rotational state j', E_{avail} is the amount of energy available, and $P^0(j',E_{\text{avail}})$ is the prior distribution, $P^0(j',E_{\text{avail}})=(2j'+1)\sqrt{E_{\text{avail}}}$. For this reaction, the amount of available energy is given by $E_{\text{avail}}=E_{\text{coll}}+E_{\text{rxn}}-E'_{\text{vib}}-E'_{\text{rot}}$, where E_{coll} is the collision energy, E_{rxn} is the reaction endoergicity (from the differences in D_2 and HD zero-point energies), and E'_{vib} and E'_{rot} are the vibrational and rotational energy above the ground state of the HD product. Figure 10 presents a linear surprisal plot for all eight collision energies. We find that the slope of the lines (the surprisal parameter θ) becomes smaller at higher collision energies, indicating that the distributions become more statistical. A similar result has been seen in previous theoretical work on this reaction and is to be expected as reactions generally behave more statistically at higher collision energies.[71] This analysis indicates that constraints besides energy conservation play an important role at low energies but those constraints are less important at higher energies. We also perform a surprisal analysis on the distributions resulting from time-dependent calculations; in Table III we compare the surprisal parameters derived from experiment and from theory. As seen in the experimental data, the calculated distributions behave more statistically at higher energies. However, the surprisal parameters are consistently smaller for the experimental data than for the theoretical results; in other words, the experimental distributions are more statistical than the theoretical ones. This discrep-

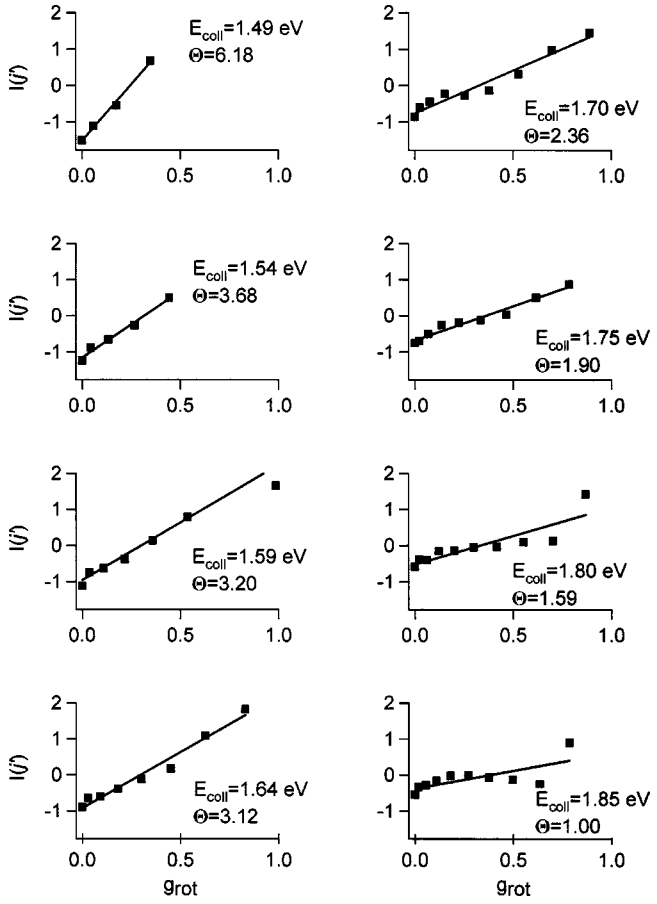

FIG. 10. Linear surprisal analysis of the experimental rotational distributions at each collision energy. The x axis is the reduced rotational energy, $g_{\text{rot}}=E'_{\text{rot}}/(E_{\text{avail}}-E'_{\text{vib}})$.

TABLE III. Experimental and theoretical linear surprisal parameters as a function of collision energy.

E_{coll} (eV)	$\theta_{\text{experimental}}$	$\theta_{\text{theoretical}}$
1.49	6.18	7.27
1.54	3.68	6.94
1.59	3.20	5.82
1.64	3.12	5.53
1.70	2.36	5.06
1.75	1.90	4.48
1.80	1.59	3.79
1.85	1.00	2.67

ancy worsens at higher collision energies, so this analysis restates the systematic disagreement between theory and experiment.

Whenever a disagreement occurs between theory and experiment, possible errors in the experiment, the theory, or both must be considered. We have demonstrated our ability to measure experimentally the relative population of $HD(\nu'=3,j')$ states for a rotationally thermal distribution. We also have shown that the experiment has no bias toward detection of any particular laboratory frame velocity and that the measured distributions do not depend on the time delay between initiation and detection. Although we have no experimentally determined line strengths for REMPI transitions with $j>4$, we trust the analysis because of the past close agreement with theoretically calculated line strengths that show a weak dependence on j. Given these and other checks, we are confident in our ability to measure rotational distributions for this reaction. Thus, we believe that the cause of the disagreement most likely arises in the theory.

We have also shown excellent agreement between two different QM theoretical methods, indicating that the dynamics on the surface are being treated correctly within the stated approximations. Indeed, it should be emphasized that, in addition to using two completely different methods to solve the Schrödinger equation, these two sets of calculations represent the (electronic ground state) Hamiltonian using completely different coordinate systems and basis functions. Hence, the close agreement between the two sets of results demonstrates that the nuclear dynamics calculations are free from numerical errors. By simulating the spread of collision energies and distributions of D_2 rotational states present in the experiment, we believe the calculations appropriately model the experimental conditions. Therefore, it seems most likely that the error originates either in the adiabatic potential surface or in dynamical effects ignored in both QM treatments, for example, non-Born-Oppenheimer effects.

The BKMP2 potential surface[33] is employed in all calculations carried out in this work. While this surface has been shown to be quite reliable,[16,72] these experiments are run at higher energies than previous measurements of rotational distributions, so these distributions are sensitive to high-energy parts of the potential energy surface that are irrelevant at lower energies; however, differential cross-section measurements at even higher energies have been in good agreement with adiabatic QM calculations on this surface.[73,74] In addition to errors in the surface, the discrepancy may result from geometric phase effects. Trajectories that encircle the conical intersection in this system acquire an additional phase factor known as geometric phase,[75–77] but this effect has been ignored in both sets of QM calculations. Much previous work on the hydrogen exchange reaction has shown quantitative agreement with theoretical results that ignore the geometric phase effect. However, arguments have been presented that geometric phase influences rotational distributions in this reaction,[37–39] although those results are being questioned and debated.[78–81] Regardless, the geometric phase certainly exists, and its neglect may well contribute to this disagreement between theory and experiment. In addition, it has recently been demonstrated that inclusion of the Born–Oppenheimer diagonal correction is required to model the kinetics of $H+H_2$ at low temperatures.[29] That correction is omitted in these calculations, and it also may contribute to the discrepancy. Although the results are still preliminary, we note that measurements and time-dependent calculations of rotational distributions for the $\nu'=2$ manifold of this reaction agree over a range of collision energies similar to those discussed here. If these results are confirmed, they would serve as further validation of the accuracy of both the experiment and the calculations, deepening the mystery of the disagreement for the $\nu'=3$ manifold.

VI. CONCLUSION

We have presented measurements of rotational distributions for the reaction $H+D_2 \rightarrow HD(\nu'=3,j')+D$ as a function of collision energy over the range 1.49–1.85 eV, and we have combined these distributions with a previous measurement[45] of the excitation function for the reaction $H+D_2 \rightarrow HD(\nu'=3,j'=0)+D$ to produce an $E-j'$ plot for this reaction. A surprisal analysis shows that the distributions become more statistical at higher energies, as is expected from previous theoretical results and on more general grounds.[71] We also compare the experimental results to both time-independent and time-dependent QM calculations on the BKMP2 potential energy surface. While these two disparate theoretical methods agree extremely well with each other, they fail to reproduce many of the experimental rotational distributions. In particular, the calculated distributions become systematically too cold, when compared to experiment, at increasing collision energies. This discrepancy is recast in other terms by conducting a surprisal analysis of the theoretical results: comparing the experimentally versus theoretically derived surprisal parameters shows that theory is consistently less statistical than experiment, with that difference being more prominent at high collision energies. We propose that this discrepancy likely results from deficiencies in the adiabatic potential energy surface or from the neglect of nonadiabatic effects in the calculations or from both. Not surprisingly, when discrepancies of this type arise, it is easy to conclude that more work is still needed to understand this simplest of all neutral bimolecular reactions.

ACKNOWLEDGMENTS

We are grateful to H. A. Bechtel, D. J. A. Brown, and J. P. Camden for critical proofreading. S.C.A. thanks the Royal Society for a University Research Fellowship. J.F.C. gratefully acknowledges financial support from the Spanish Ministry of Science and Technology through a contract within the *Ramon y Canal* program. The Spanish group was supported by the Spanish Ministry of Science and Technology (Project No. BQU2002-04627-C02-02) and by the European Commission within the RT Network *Reaction Dynamics* (Contract No. HPRN-CT-1999-00007). The American group expresses its gratitude to the National Science Foundation that supported this work under NSF CHE 02-42103.

[1] F. London, Z. Elektrochem. Angew. Phys. Chem. **35**, 552 (1929).
[2] H. Eyring and M. Polanyi, Z. Phys. Chem. Abt. B **12**, 279 (1931).
[3] E. E. Marinero, C. T. Rettner, and R. N. Zare, Phys. Rev. Lett. **48**, 1323 (1982).
[4] J. J. Valentini, in *Spectrometric Techniques*, edited by G. A. Vanasse (Academic, New York, 1985), Vol. 4, p. 1.
[5] D. P. Gerrity and J. J. Valentini, J. Chem. Phys. **79**, 5202 (1983).
[6] R. E. Continetti, B. A. Balko, and Y. T. Lee, J. Chem. Phys. **93**, 5719 (1990).
[7] L. Schnieder, W. Meier, K. H. Welge, M. N. R. Ashfold, and C. M. Western, J. Chem. Phys. **92**, 7027 (1990).
[8] L. Schnieder, K. Seekamp-Rahn, F. Liedeker, H. Steuwe, and K. H. Welge, Faraday Discuss. Chem. Soc. **91**, 259 (1991).
[9] T. N. Kitsopoulos, M. A. Buntine, D. P. Baldwin, R. N. Zare, and D. W. Chandler, Science **260**, 1605 (1993).
[10] N. E. Shafer, H. Xu, R. P. Tuckett, and M. Springer, J. Phys. Chem. **98**, 3369 (1994).
[11] H. Xu, N. E. Shafer-Ray, F. Merkt, D. J. Hughes, M. Springer, R. P. Tuckett, and R. N. Zare, J. Chem. Phys. **103**, 5157 (1995).
[12] K. Liu, Annu. Rev. Phys. Chem. **52**, 139 (2001).
[13] D. P. Gerrity and J. J. Valentini, J. Chem. Phys. **81**, 1298 (1984).
[14] H. B. Levene, D. L. Phillips, J. Nieh, D. P. Gerrity, and J. J. Valentini, Chem. Phys. Lett. **143**, 317 (1988).
[15] D. A. V. Kliner, K.-D. Rinnen, and R. N. Zare, Chem. Phys. Lett. **166**, 107 (1990).
[16] L. Bañares, F. J. Aoiz, V. J. Herrero, M. D'Mello, B. Niederjohann, K. Seekamp-Rahn, E. Wrede, and L. Schnieder, J. Chem. Phys. **108**, 6160 (1998).
[17] B. D. Bean, F. Fernández-Alonso, and R. N. Zare, J. Phys. Chem. A **105**, 2228 (2001).
[18] B. D. Bean, J. D. Ayers, F. Fernández-Alonso, and R. N. Zare, J. Chem. Phys. **116**, 6634 (2002).
[19] L. Schnieder, K. Seekamp-Rahn, E. Wrede, and K. H. Welge, J. Chem. Phys. **107**, 6175 (1997).
[20] S. C. Althorpe, F. Fernández-Alonso, B. D. Bean, J. D. Ayers, A. E. Pomerantz, R. N. Zare, and E. Wrede, Nature (London) **416**, 67 (2002).
[21] S. A. Harich, D. Dai, C. C. Wang, X. Yang, S. D. Chao, and R. T. Skodje, Nature (London) **419**, 281 (2002).
[22] D. Dai, C. C. Wang, S. A. Harich, X. Wang, X. Yang, S. D. Chao, and R. T. Skodje, Science **300**, 1730 (2003).
[23] R. Goetting, J. P. Toennies, and M. Vodegel, Int. J. Chem. Kinet. **18**, 949 (1986).
[24] D. A. V. Kliner and R. N. Zare, J. Chem. Phys. **92**, 2107 (1990).
[25] D. G. Truhlar and R. E. Wyatt, Annu. Rev. Phys. Chem. **27**, 1 (1976).
[26] H. Buchenau, J. P. Toennies, J. Arnold, and J. Wolfrum, Ber. Bunsenges. Phys. Chem. **94**, 1231 (1990).
[27] G. C. Schatz, Annu. Rev. Phys. Chem. **39**, 317 (1988).
[28] S. C. Althorpe and D. C. Clary, Annu. Rev. Phys. Chem. **54**, 493 (2003).
[29] S. L. Mielke, K. A. Peterson, D. W. Schwenke, B. C. Garrett, D. G. Truhlar, J. V. Michael, M.-C. Su, and J. W. Sutherland, Phys. Rev. Lett. **91**, 063201 (2003).
[30] D. P. Gerrity and J. J. Valentini, J. Chem. Phys. **83**, 2207 (1985).
[31] N. C. Blais and D. G. Truhlar, J. Chem. Phys. **83**, 2201 (1985).
[32] S. C. Althorpe, J. Chem. Phys. **117**, 4623 (2002).
[33] A. I. Boothroyd, W. J. Keogh, P. G. Martin, and M. R. Peterson, J. Chem. Phys. **104**, 7139 (1996).
[34] S. L. Mielke, B. C. Garrett, and K. A. Peterson, J. Chem. Phys. **116**, 4142 (2002).
[35] A. Kuppermann and G. C. Schatz, J. Chem. Phys. **62**, 2502 (1975).
[36] M. Zhao, M. Mladenovic, D. G. Truhlar, D. W. Schwenke, Y. Sun, D. J. Kouri, and N. C. Blais, J. Am. Chem. Soc. **111**, 852 (1989).
[37] D. A. V. Kliner, D. E. Adelman, and R. N. Zare, J. Chem. Phys. **95**, 1648 (1991).
[38] A. Kuppermann and Y.-S. M. Wu, Chem. Phys. Lett. **205**, 577 (1993).
[39] A. Kuppermann and Y.-S. M. Wu, Chem. Phys. Lett. **213**, 636 (1993).
[40] D. P. Gerrity and J. J. Valentini, J. Chem. Phys. **82**, 1323 (1985).
[41] J. Nieh and J. J. Valentini, J. Chem. Phys. **92**, 1083 (1990).
[42] D. A. V. Kliner, D. E. Adelman, and R. N. Zare, J. Chem. Phys. **94**, 1069 (1991).
[43] D. E. Manolopoulos and R. E. Wyatt, Chem. Phys. Lett. **159**, 123 (1989).
[44] J. Z. H. Zhang and W. H. Miller, Chem. Phys. Lett. **153**, 465 (1988).
[45] J. D. Ayers, A. E. Pomerantz, F. Fernández-Alonso, F. Ausfelder, B. D. Bean, and R. N. Zare, J. Chem. Phys. **119**, 4662 (2003).
[46] E. E. Marinero, C. T. Rettner, and R. N. Zare, J. Chem. Phys. **80**, 4142 (1984).
[47] W. M. Huo, K.-D. Rinnen, and R. N. Zare, J. Chem. Phys. **95**, 205 (1991).
[48] K.-D. Rinnen, M. A. Buntine, D. A. V. Kliner, R. N. Zare, and W. M. Huo, J. Chem. Phys. **95**, 214 (1991).
[49] A. E. Pomerantz, F. Ausfelder, R. N. Zare, and W. M. Huo (unpublished).
[50] R. I. Hall, I. Cadež, M. Landau, F. Pichou, and C. Schermann, Phys. Rev. Lett. **60**, 337 (1988).
[51] P. J. Eenshuistra, J. H. M. Bonniw, J. Los, and H. J. Hopman, Phys. Rev. Lett. **60**, 341 (1988).
[52] D. C. Robie, L. E. Jusinski, and W. K. Bischel, Appl. Phys. Lett. **56**, 722 (1990).
[53] F. Fernández-Alonso, B. D. Bean, J. D. Ayers, A. E. Pomerantz, and R. N. Zare, Z. Phys. Chem. (Munich) **214**, 1167 (2000).
[54] W. M. Huo (private communication).
[55] F. Fernández-Alonso, B. D. Bean, R. N. Zare, F. J. Aoiz, L. Bañares, and J. F. Castillo, J. Chem. Phys. **115**, 4534 (2001).
[56] D. A. Dahl, SIMION 3D, U.S. Department of Energy, Office of Energy Research, Idaho Falls, 1995.
[57] P. M. Regan, S. R. Langford, A. J. Orr-Ewing, and M. N. R. Ashfold, J. Chem. Phys. **110**, 281 (1999).
[58] S. C. Althorpe, J. Chem. Phys. **114**, 1601 (2001).
[59] D. Skouteris, J. F. Castillo, and D. E. Manolopoulos, Comput. Phys. Commun. **133**, 128 (2000).
[60] F. J. Aoiz, L. Bañares, and V. J. Herrero, J. Chem. Soc., Faraday Trans. **94**, 2483 (1998).
[61] L. Bañares, F. J. Aoiz, P. Honvault, B. Bussery-Honvault, and J.-M. Launay, J. Chem. Phys. **118**, 565 (2003).
[62] F. Fernández-Alonso, B. D. Bean, and R. N. Zare, J. Chem. Phys. **111**, 1022 (1999).
[63] N. C. Blais and D. G. Truhlar, Chem. Phys. Lett. **102**, 120 (1983).
[64] R. S. Blake, K. Rinnen, D. A. V. Kliner, and R. N. Zare, Chem. Phys. Lett. **153**, 365 (1988).
[65] K.-D. Rinnen, D. A. V. Kliner, R. S. Blake, and R. N. Zare, Chem. Phys. Lett. **153**, 371 (1988).
[66] N. C. Blais and D. G. Truhlar, Chem. Phys. Lett. **162**, 503 (1989).
[67] C. A. Picconatto, A. Srivastava, and J. J. Valentini, J. Chem. Phys. **114**, 1663 (2001).
[68] J. J. Valentini, J. Phys. Chem. A **106**, 5745 (2002).
[69] R. D. Levine and R. B. Bernstein, Acc. Chem. Res. **7**, 393 (1974).
[70] R. D. Levine and R. B. Bernstein, *Molecular Reaction Dynamics and Chemical Reactivity* (Oxford University Press, New York, 1987).
[71] E. Zamir, R. D. Levine, and R. B. Bernstein, Chem. Phys. Lett. **107**, 217 (1984).
[72] F. Fernández-Alonso and R. N. Zare, Annu. Rev. Phys. Chem. **53**, 67 (2002).
[73] E. Wrede, L. Schnieder, K. H. Welge, F. J. Aoiz, L. Bañares, V. J. Herrero, B. Martínez-Haya, and V. Sáez Rábanos, J. Chem. Phys. **106**, 7862 (1997).
[74] E. Wrede, L. Schnieder, K. H. Welge, F. J. Aoiz, L. Bañares, J. F. Castillo, B. Martínez-Haya, and V. J. Herrero, J. Chem. Phys. **110**, 9971 (1999).
[75] M. V. Berry, Proc. R. Soc. London, Ser. A **392**, 45 (1984).
[76] Y.-S. M. Wu, A. Kuppermann, and B. Lepetit, Chem. Phys. Lett. **186**, 319 (1991).
[77] A. Kuppermann, in *Dynamics of Molecules and Chemical Reactions*, edited by R. E. Wyatt and J. Z. H. Zhang (Dekker, New York, 1996), 411 pp.
[78] B. K. Kendrick, J. Chem. Phys. **112**, 5679 (2000).
[79] B. K. Kendrick, J. Chem. Phys. **114**, 4335 (2001).
[80] A. Kuppermann and Y.-S. M. Wu, Chem. Phys. Lett. **349**, 537 (2001).
[81] B. K. Kendrick, J. Chem. Phys. **118**, 10502 (2003).